Enhanced SEA algorithm and fingerprint classification

Li Min Liu*

Department of Applied Mathematics,
Chung Yuan Christian University,
Chung-Li, Taiwan, ROC
E-mail: lmliu@math.cycu.edu.tw
*Corresponding author

Ching Yu Huang

Center for Pharmacogenomics and Complex Disease Research,
New Jersey Dental School, Newark, NJ 07101, USA
E-mail: austin.huang@umdnj.edu

Tian Shyr Dai

Department of Information and Financial Management,
National Chiao-Tung University, Hsin-Chu, Taiwan, ROC
E-mail: cameldai@mail.nctu.edu.tw

George Chang

Department of Mathematics and Computer Science,
Kean University, Union, NJ 07083, USA
E-mail: gchang@kean.edu

Abstract: This paper proposes the Enhanced Shrinking and Expanding Algorithm (ESEA) with a new categorization method. The ESEA overcomes anomalies in the original Shrinking and Expanding Algorithm (SEA) which fails to locate singular points (SPs) in many cases. Experimental results show that the accuracy rate of the ESEA reaches 94.7%, a 32.5% increase from the SEA. In the proposed fingerprint categorization method, each fingerprint will be assigned to a specific subclass. The search for a specific fingerprint can therefore be performed only on specific subclasses containing a small portion of a large fingerprint database, which will save enormous computational time.

Keywords: fingerprint; fingerprint classification; singular points; SPs; fault line; directional image.

Reference to this paper should be made as follows: Liu, L.M., Huang, C.Y., Dai, T.S. and Chang, G. (xxxx) 'Enhanced SEA algorithm and fingerprint classification', *Int. J. Computer Applications in Technology*, Vol. x, No. x, pp.xxx–xxx.

Biographical notes: L.M. Liu received his PhD in Computer and Information Science from New Jersey Institute of Technology in 1999. He is currently an Assistant Professor in the Department of Applied Mathematics at Chung Yuan Christian University (Taiwan). His current research interests include fingerprint technologies, image processing OO modelling, and computer-assisted language learning.

C.Y. Huang is currently a Senior Computer Scientist at the Center for Pharmacogenomics and Complex Disease Research (CPCDR), New Jersey Dental School, University of Medicine and Dentistry of New Jersey (UMDNJ). He holds BSc in Computer Sciences from TamkangUniversity, and received his MSc and PhD in Computer and Information Sciences at New Jersey Institute of Technology (NJIT). His research interests are in image processing, pattern recognition, bioinformatics, cluster analysis, genotyping methods and QC, and application developments.

T.S. Dai is currently an Assistant Professor at the Department of Information and Financial Management of the National Chiao-Tung University (Taiwan). He obtained his PhD in the Department of Computer Science and Information Engineering at National Taiwan University, Taiwan. His research interests are in financial engineering and algorithms.

George Chang is an Associate Professor in the Mathematics and Computer Science Department at Kean University. He received his BSc in Computer Science and Applied Mathematics and Statistics from SUNY Stony Brook, and his MSc and PhD in Computer and Information Science from New Jersey Institute of Technology. He is the lead author of the book *Mining the World Wide Web – An Information Search Approach*, Kluwer Academic Publishers, 2001 (Japanese language translation published 2004) and has authored many journal and conference publications. His research interests include databases, bioinformatics systems, data mining, information retrieval, and high-performance computing.

1 Introduction

Fingerprint analysis is probably one of the oldest and most commonly used identification technologies in biometrics. Identifying a fingerprint against a huge database can be extremely time-consuming, which may be considered unacceptable in many fields, especially in criminal investigation. If fingerprints can be properly pre-assigned into classes, then the searching process can be performed only on the associated classes instead of the entire database, which will then significantly reduce computational time.

In the early 20th century, Henry (1900) had categorised fingerprints into three basic types: *loop*, *arch* and *whorl*. The *loop* type was then further subcategorised into *left loop* and *right loop*, and the *arch* type was subdivided into *plain arch* (or *arch* for short) and *tented arch*. This 5-class classification system has been adopted by the National Institute of Standards and Technology (NIST) special database 4, NIST-4 (Watson and Wilson, 1992). A typical fingerprint for each class is illustrated in Figure 1. For convenience, we use the letter '*A*' for *arch*, '*T*' for *tend arch*, '*L*' for *left loop*, '*R*' for *right loop*, and '*W*' for *whorl*.

Figure 1 The Henry patterns: (a) arch; (b) tented arch; (c) right loop; (d) left loop and (e) whorl with a circle shape ridge flows in the centre

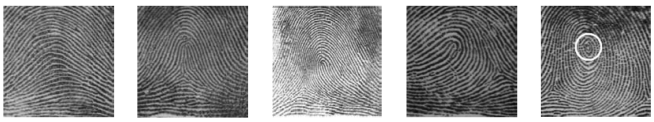

(a) (b) (c) (d) (e)

Another well known and the most complicated classification system is the National Crime Information Center (NCIC) classification system (Federal Bureau of Investigation, 1984) which includes 19 classes. The NCIC classification system has been adopted by the NIST-9 and NIST-14 databases. The NCIC defines two arch types, *Arch* and *Tented Arch*, which are identical to the Henry system, and two loop types, *Radial* and *Ulnar*, where the radial/ulnar loops towards the thumb/little finger. Whorl type is subdivided into four types: *Plain Whorl*, *Central Pocket Whorl*, *Double Loop Whorl*, and *Accidental Whorl*. Each whorl type has three subcategories depending on the ridge tracing: Inner, Outer, and Meeting. The last three types are *Approximate Class*, *Amputation*, and *Scar*. Figure 2 shows some examples of the NCIC classification system.

Figure 2 Some of the NCIC classes: (a) plain whorl (inner); (b) central pocket whorl (inner); (c) double loop whorl (inner); (d) accidental whorl (inner) and (e) scar; 'Δ' and 'O' marked in (a) denote two types of SP the delta and the core, respectively

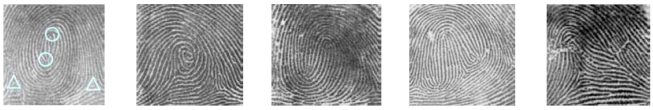

(a) (b) (c) (d) (e)

In the last few decades, many Automated Fingerprint Identification System (AFIS) (Jain et al., 1999) applications and algorithms have been developed with the help of high performance computers. Computers have gradually replaced human experts in performing fingerprint classification and recognition. Most researchers adopt Henry's 5-class classification system to verify the performance of their classification algorithms. Meanwhile, various classification algorithms have been built based on a 4-class system (R, L, W, and AT) by combining *Arch* and *Tented Arch* named 'AT' (Jain and Minut, 2002; Senior, 2001). We have not found any algorithm based on the NCIC system. According to the techniques used, these algorithms can be categorised into two groups: *flat* and *structural* (Marcialis et al., 2001). Researchers using the 'flat' approach favour statistical patterns (Jain et al., 1999). Karu and Jain (1996) used the number and locations of the Singular Points (SPs), Jain et al. (1999) used 192-dreictional FingerCodes, and Neto and Borges (1997) applied the Hidden Markov Models. The 'structural' approach introduced by Cappelli et al. (1999) uses syntactic patterns to categorise fingerprints. Yao et al. (2003) proposed an approach based on two machine learning algorithms: Support Vector Machines and Recursive Neural Networks with an integration of flat and structural representations. However, some problems exist for these methods. For instance, in the flat approach, it is not easy to detect SPs, and the uncertainty in the location of SPs is high. On the other hand, the information provided by the structural approach is not sufficient for differentiating the '*L*', '*R*', and '*T*' types of fingerprints (Tan et al., 2003).

Each fingerprint consists of two special direction-oriented parts, ridges and valleys, which constitute two major characteristics: a set of global features called *singular points* and a set of local features named *minutiae*. SPs represent regional directional makeup and can be divided into two types: *core* and *delta*. A core/delta point is defined as a concentrate region where the ridge curvature is converging to a local maximum/minimum (Srinivasan and Murthy, 1992). For example, two delta points and two core points are marked by 'Δ' and 'O' respectively in Figure 2(a). Minutiae are local deformation of the ridges such as 'ridge ending' or 'bifurcation'. A constructive definition for minutiae can be found in Bolle et al. (2002).

Correctly locating SPs is crucial for most fingerprint related applications. To locate SPs, two popular approaches, the Poincaré index (Kawagoe and Tojo, 1984) and the directional image, are introduced (Grasselli, 1969; Sherlock and Monro, 1993). One important problem of the former approach is that the Poincaré index calculation is very sensitive to noise and may lead to detection of false SPs. Sherlock and Monro (1993) used directional images based on 16×16 pixel blocks to describe the topological behaviour of ridge flows around the SPs. The algorithm described in Yao et al. (2003) constructs the directional images by 28×30 matrices. The two drawbacks of using block direction are that directional images suffer from

- poor contrast (Hong et al., 1998)
- loss of details of ridges (Srinivasan and Murthy, 1992).

Furthermore, if a '*W*' type fingerprint has a nearly perfect circle in the middle area as shown in Figure 1(e), a block-based directional image will indicate one core 'region' in the middle, which is different from Figure 2(a) with two core regions due to the oval-shaped ridge flows. Huang et al. (2007) proposed the SEA based on pixel-wised directional images to locate SPs in a 2×2 pixel area. The SEA is one of the pioneer algorithms which can locate SPs in a small area and properly eliminate false SPs by reducing image resolution.

However, our experimental results have shown that the SEA fails to locate SPs on many fingerprints. Such failure is basically due to the following two problems: "*The Valid Singular Point Disappearing Problem*" and "*The Narrow Arch Anomaly*". The proposed ESEA can overcome these problems and properly locate SPs by building a different shrinking pyramid from the SEA with a pixel validation mechanism which is not included in the original SEA. We also present a simple quantitative fingerprint classification scheme based on the type and number of SPs. Distances among SPs are used for sub-classification purpose. In this scheme, fingerprint images can be grouped into as many subclasses as the users wish. Thus, identifying a fingerprint from a huge database can be done by searching particular subclasses only instead of the entire database.

The rest of the paper is organised as follows. Section 2 describes the proposed fingerprint classification and the SEA. Section 3 shows the problems of SEA, followed by the ESEA in Section 4. The proposed sub-classification scheme is described in Section 5. Finally, the conclusions are presented in Section 6.

2 Fingerprint classification by Singular Points (SPs)

2.1 Classification by SP pairs

Current fingerprint classification systems, including Henry and NCIC, categorise fingerprints by analysing the relationship between ridge flows and SPs. Such systems require complicated algorithms. The proposed classification system is easier to apply by using the number of SP pairs to categorise fingerprints. Ideally, '*A*' type fingerprints have no SPs. '*R*', Figure 3(a), ('*L*', Figure 3(b)) type fingerprints have the core point appearing on top-right (top-left) of the delta point, and the ridge flows around the core point are directing to bottom-right (bottom-left). '*T*' type fingerprints, Figure 3(c), have the core point appearing on top of the delta point with near symmetric ridge flows on two sides of the core-delta line. In other words, types '*R*', '*L*', and '*T*' have exactly one core and one delta (one core-delta pair, or 1 SP pair in short). '*W*' type fingerprints have 2 SP pairs as shown in Figure 3(d) and (e). Figure 3(f) shows an *Accidental Whorl* fingerprint in the NCIC system with three SP pairs. Instead of classifying fingerprints by analysing the detail ridge flow, we propose a simple classification system based on the number of SP pairs, where a fingerprint type is defined as: FT_i with i SP pair(s), where $0 \le i \le 3$.

Figure 3 (a)–(c) are in FT_1; (d) and (e) are in FT_2 and (f) is in FT_3

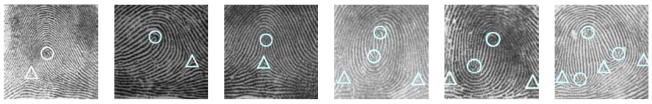

(a) (b) (c) (d) (e) (f)

The proposed classification system has two advantages over Henry's or NCIC classifications. First, it is simple and straightforward. Second, the classification scheme can reduce the number of fingerprints required to compare with during the recognition process. As a matter of fact, there exist many fingerprints that belong to multiple types. For instance, the NIST-4 database contains 23% (946/4000) of images that belong to two types. In other words, searching for such an example requires examining both types in the database. By combining '*R*', '*L*', and '*T*' together to FT_1, nearly half of the double typed images (496/946) will be grouped together. Then the searching process can be performed only on type FT_1 rather than two types. However, fewer fingerprint types lead to more images in each class. Therefore, it is essential to further divide each class into subclasses to reduce the number of images within each subclass. The proposed sub-classification scheme is able to dynamically divide the class into a specific number of subclasses or into subclasses with a specific number of fingerprints. This ability can reduce the number of images required for comparison during the recognition process,

which is what Henry's classification system is unable to achieve. The sub-classification scheme will be explained in a later section.

2.2 Singular Points (SPs) analysis

In order to make the proposed classification system work, the number and type of SPs must be properly derived, and a SP has to be defined in a relatively small area. The SEA is based on pixel-wised directional images using the quantification function to map the range of angle $[0, \pi)$ to an integer in the range of $[0, N-1]$. Each pixel, P, will be assigned to one of these N directions according to the flow orientation in a circle with radius w and centred at P. To visualise the directional image, we colour the directions in grey scale – black for 0 and white for $N-1$ as shown in Figure 4. The rest of the directions are represented by various scales of grey, each called a *direction zone*. A direction zone of direction number n is denoted as $\Omega(n)$. $CM(N, w)$ represents different combinations of quantification range and active circle region size. The complexity of calculating the flow orientation of P is $O(w^2)$. For a fingerprint image FI with $width \times height$ pixels, the complexity of generating the pixel-wised directional image of FI is $O(width \times height \times w^2)$.

Figure 4 (a) and (b) are directional images of Figure 3(a) with $CM(3, 5)$ and $CM(4, 5)$; (c) and (d) show the fault lines of (a) and (b); (e) two directional sequences

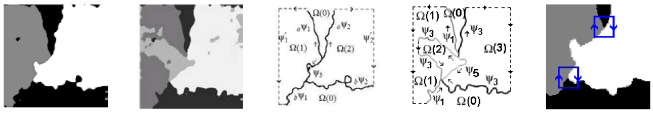

(a) (b) (c) (d) (e)

A *fault line* Ψ_{i+j} is then defined as the separating boundary between two adjacent directional zones $\Omega(i)$ and $\Omega(j)$. Figure 4(a) and (b) show the directional images of the fingerprint shown in Figure 3(a) with different parameter combinations, and Figure 4(c) and (d) show the fault lines of (a) and (b), respectively. When $N = 3$, three directions, 0 degree (or 0), 60 degrees (or 1), and 120 degrees (or 2), will be considered, and they will be represented by black, grey, and white, respectively. For the sake of easy understanding, direction 0, 1, 2 will be assigned to pixels with slopes ranging from [–30, +30), [+30, +90), and [+90, 150), respectively. A SP is defined as the block which contains a SP directional sequence. The clockwise directional sequence for a core (delta) is $0 \to 2 \to 1 \to 0$ ($0 \to 1 \to 2 \to 0$). For example, Figure 4(e) contains two 10×10 blocks with 38 border pixels. The clockwise directional sequence of the top block is black → white → grey → black (or $0 \to 2 \to 1 \to 0$), indicating a core point exists in this block and can be defined in a 2×2 pixel area by reducing the block size. More details about fault line analysis can be found in Huang et al. (2007). Figure 5 shows the pixel-wised directional images of Figure 2(a)–(d). SPs are clearly presented on these directional images. For a *Central Pocket Whorl* fingerprint as shown in Figure 5(b), the directional image shows two core points, and the distance between them is less than three ridge-valley width (24 pixels). Most block-based algorithms will consider such a case as having only one core 'region' and therefore cannot provide proper information about SP pairs.

Figure 5 Pixel-wised directional images of Figure 2(a)–(d)

(a) (b) (c) (d)

2.3 Shrinking and Expanding Algorithm (SEA)

The pixel-wised directional image is created from calculation results based on individual pixels. Calculation results from any single noise pixel may create a false SP, since a SP block can be as small as 2×2. To correctly detect the coordinates of SPs, a two-phased SEA based on a scale-pyramid is presented in Huang et al. (2007). The basic idea is that scaling down the image resolution eliminates noise-introduced SPs and retains valid SP candidates. To perform the scale-down, a directional image I_k is first divided into a grid of units with $r \times r$ pixels in size where r is the shrinking factor. Each unit is represented by only one pixel in the next level directional image, denoted as I_{k+1}, with its value set to be the dominate direction of the $r \times r$ grid. The noise reduction effort can be clearly observed as the image scale-down level by level. An example of a scale pyramid in shrinking phase is shown in Figure 6(a)–(d). In such an example, the pyramid is created with four levels with the original direction image I_0 on the bottom and I_3 on the highest level. It is hard to decide when to stop the scale-down process. If it stops too early, the noise level will still be too high. However, if we scale-down too much, directional sequences from valid SPs might be eliminated in the process. To resolve this dilemma, Huang et al. (2007) suggested that the combination of shrinking factor and the level of scale-pyramid should be 3 and 4.

Figure 6 Scale-pyramid in shrinking phase with $r = 3$: (a) I_0; (b) I_1; (c) I_2 and (d) I_3, and in expanding phase (e) I_0; (f) I_1; (g) I_2 and (h) I_3

(a) (b) (c) (d)

The second phase (or expanding phase) is to search for SP candidates starting from the top level of the scale-pyramid. First identify SP candidates in a 2×2 area at level I_3. For every candidate found at level I_3, we subsequently search the associated $2r \times 2r$ area at the next lower level I_2. This procedure is performed until level I_0 is reached. An example of a scale pyramid in expanding phase is shown

in Figure 6(h)–(e). The boxes show candidates identified at a particular level. The complexity of generating the SEA pyramid and searching for the SP candidate are both $O(width \times height)$, which is smaller than the complexity of generating pixel-wised directional image $O(width \times height \times w^2)$. Hence, the overall complexity of the SEA is $O(width \times height \times w^2)$.

3 Problems of the SEA

3.1 The valid singular point disappearing problem

The number of SPs might decrease when we move from a lower level to a higher level in the SEA pyramid because of the resolution reduction. Ideally, resolution reduction should only eliminate noise-introduced SPs, and the top level of the scale-pyramid should retain all valid SPs. However, if two SPs are closely connected by a small island-shaped direction zone, the SP sequences will not be retained after a few steps of resolution reduction. This is called the "*Valid Singular Point Disappearing Problem*". Figure 7 illustrates such an example where (b) is the binarised image of (a), and (c) shows the directional image I_0 of (b) with four SPs appearing on it. Figure 7(d) is the top level image I_3 with only two SPs.

Figure 7 (b) is the binarised image of (a); (c) is the directional image of (b); the valid SP disappears after two times of resolution reduction in (d)

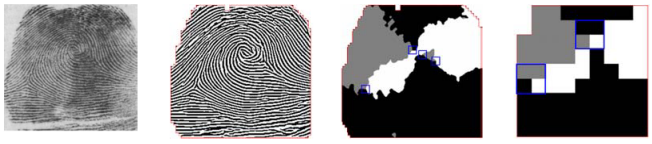

(a) (b) (c) (d)

In such a case, valid SPs do not appear on the top SEA pyramid. The level at which these valid SPs disappear depends on the size of the particular small island-shaped direction zone. If the size of such an island is small, valid SPs might be eliminated after several times of shrinking processes, suggesting that the ideal starting searching level should be relatively low. However, noise-introduced SPs might still be present if the starting searching level is set too low.

3.2 The Narrow Arch Anomaly

Another problem is that SPs identified at a higher level do not have associated SPs at a lower level. We called this problem the '*Narrow Arch Anomaly*'. Figure 8 illustrates such an example where (b) is the binarised image of (a), and (c) is the directional image of (b). The resolution reduced images (Figure 8(d) and (e)) do indicate two SPs appearing on this fingerprint. However, if we move down a few levels, we cannot locate the associated SPs. The SPs identified at a higher level are not created by noises but resolution reduction. This anomaly contradicts the assumption that the number of SP decreases when we travel upward in the SEA pyramid.

Figure 8 (b) is the binarised image of (a); higher pyramid levels (d) and (e) Identified SPs, but do not have associated SPs at lower level (c)

(a) (b) (c) (d) (e)

4 Enhanced Shrinking and Expanding Algorithm (ESEA)

These two problems suggest that the starting searching level within the scale pyramid should not be set too high. However, if the starting searching level is too low, noise-introduced SPs may not be eliminated. To resolve this dilemma, we developed an enhanced version of the original SEA (ESEA). The direction of pixel (i, j) at ESEA pyramid level k, $I_{k(i,j)}$, is defined as follows:

$$I_{k(i,j)} = \mathrm{Dom}((i \times F_k, j \times F_k), ((i+1) \times F_k - 1, (j+1) \times F_k - 1)), \quad (1)$$

F_k equals $f \times k$ where the shrinking factor is denoted as f. I^w and I^h are the width and height of the binarised image. Function *Dom* returns the dominate direction of the square with top-left pixel at $(i \times F_k, j \times F_k)$ and bottom-right pixel at $((i+1) \times F_k - 1, (j+1) \times F_k - 1)$ on I_0.

The generation function for ESEA pyramid shown in equation (1) is identical to the one for SEA pyramid except the F_k in SEA is defined as f^k. The search for SPs starts from the top level, I_w, of the ESEA pyramid, and we consider only pixels with a 'valid' flag and ignore pixels with an 'ignored' flag. Let p be a pixel located at (i, j), c be the centre point of the minimum rectangle which can cover the foreground fingerprint image, m be the length of the short edge of the rectangle, and dist(p, c) be the distance between p and c. The validation flag of p at a level k, $V_{k(p)}$, is defined as follows:

$$V_{k(p)} = \begin{cases} \text{valid} & \text{if } 2m_t - \delta < \mathrm{dist}(p,c), \text{ where } k = w \quad \text{OR} \\ & \text{if } \mathrm{dist}(p,c) < m_t + \delta, \text{ where } k = 2 \quad \text{OR} \\ & \text{if } m_t + (k-2)M_t - \delta < \mathrm{dist}(p,c) \\ & \quad < m_t + (k-1)M_t + \delta, \text{ where } 2 < k < w, \\ \text{ignored}, & \text{otherwise} \end{cases} \quad (2)$$

where δ is a positive constant, m_t is one third of m, and M_t is $m_t/(w-2)$. SPs identified in the valid region of a certain level will be used as anchors to find the associated SPs at a lower level. SPs found in ignored region will be considered as false SPs which will be excluded.

Figure 9(a) illustrates the directional image I_0 of Figure 7 where the border box indicates the minimum rectangle covering the foreground fingerprint image, and the centre point c is defined as the joint point of the two cross lines. The second level, I_1, and third level I_2 of the

ESEA pyramid for this fingerprint are shown in Figure 9(b) and (c), and the rest, I_3–I_5, are shown in Figure 10. Similar to Figure 7(d) and 10(c) has only two SPs, since two SPs are eliminated due to the "*Valid Singular Point Disappearing Problem*". The SP discovery process starts from I_5 where we check only the region outside the circle because the pixels inside the circle have validation flags marked as 'ignored'. One SP candidate is identified on I_5 which will be used as the anchor for locating the associated SP on the next level, I_4. In the mean time, we check pixels between these two circles for extra SPs. In this case, there is none. If we repeat this process on level I_3, three additional SPs will be identified.

Figure 9 The directional images of Figure 7; (a) I_0, (b) I_1 and (c) I_2

(a) (b) (c)

Figure 10 Resolution reduced images (a) I_3 to (d) I_5

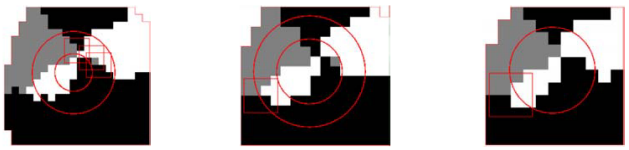

(a) (b) (c)

The identified SPs on one level will have marks on a lower level image as well. More precisely, there will be four SPs marked on I_2. These four candidates will be used to find the exact 2 × 2 locations of SPs on I_0 through I_1. This example shows that the ESEA successfully overcomes *the valid singular point disappearing problem*.

More precisely, the starting searching level in the ESEA is not fixed. The border region of an image has a higher starting level, and the centre region of an image has a lower starting level. The closer the pixel is to the centre of an image, the higher resolution we shall use. This design can properly overcome both problems described in the previous section. Furthermore, the theoretical complexity of the ESEA is the same as that of the SEA because the bottleneck of this algorithm is still at the construction of the pixel-wised directional image. However the practical complexity of the ESEA is better than that of the SEA. This is because only blocks in the valid region require checking the existence of directional sequence, and the number of examined blocks in the ESEA pyramid is smaller than that in the SEA pyramid.

4.1 Experiments

We used the NIST-4 database (4000 images) to evaluate the ESEA with our 4-class classification system. When the ESEA found no SP on a fingerprint, it was assigned to type FT_0. When one SP pair, two SP pairs, or three SP pairs were identified, it was assigned to type FT_1, FT_2, or FT_3, respectively. Tables 1 and 2 show the classification results of the original SEA and ESEA, respectively. In both tables, the rows represent data generated by each program, and the columns represent classification assigned by the NIST.

Table 1 Classification result by the SEA

SEA \ NIST	FT_0	FT_1	FT_2	FT_3
FT_0	571	129	120	0
FT_1	122	1349	885	0
FT_2	25	231	568	0
FT_3	0	0	0	0

Table 2 Classification result by the ESEA

ESEA \ NIST	FT_0	FT_1	FT_2	FT_3
FT_0	836	102	2	0
FT_1	45	2138	47	0
FT_2	0	11	720	0
FT_3	0	0	0	0

The accuracy rate of SEA is 62.2% (or 2488/4000) without any rejection, and the highest level of the SEA pyramid still contains many noise-introduced SPs, since 885 FT_1 fingerprints have been *misclassified* to FT_2. On the other hand, 231 FT_2 fingerprints have been *misclassified* to FT_1 due to *the valid singular point disappearing problem*. The experimental results show the ESEA can not only eliminate noise-introduced SPs, but also overcome both aforementioned problems to achieve a 94.7% (or 3694/3901) accuracy rate with 2.5% (or 99/4000) rejection. We rejected images with only one core or delta point as shown in Figure 11(a) and smudged images as shown in (b) and (c) where substantial portions of the images are cut-off after segmentation step. In this experiment, the ESEA pyramid has six levels (I_0–I_5). Many fingerprint images were still misclassified, as shown in Table 2, due to various reasons such as poor quality of images, small regional noise on fingerprints, or the centre of fingerprint residing on border of fingerprint images. Furthermore, since ESEA only eliminates spurious SPs and will not create any new SPs, no fingerprint classified into correct type by SEA was misclassified by ESEA.

Figure 11 Examples of rejected images: (a) one core image; (b) and (c) are smudged images

(a) (b) (c)

5 Sub-classification by distance of Singular Points (SPs)

5.1 Distance among Singular Points (SPs)

According to the type distribution statistics in the NIST-9, around 65% of the fingerprints are *loop*; 27% are *whorl*; *arch* accounts for 4% and *tented arch* accounts for 3% of the fingerprints. The NCIC system records the ridge counts between core and delta for loop type fingerprints, which can be used to reduce the number of images searched. However, the width of a ridge is not fixed for a fingerprint, and sometimes the ridge count is hard to define due to noises or minutiae. Furthermore, the angle between directions of ridge flow and delta-core vector may influence the ridge count. If we assume the distance between the core and delta of a FT_1 fingerprint is d, the ridge count can be d/(average ridge-valley width) when the ridge flow is orthogonal to the core-delta vector, or it can be 0 when the ridge flow is parallel to the core-delta vector, i.e., *tented arch* fingerprints. Hence, we believe the distance scaled in pixels provides more accurate information than ridge counts.

In our classification system, every fingerprint will be attached with a set of distance values among SPs. Since a FT_0 fingerprint has no SPs, no distance value will be attached. A FT_1 fingerprint has exactly one SP pair. Therefore, each FT_1 fingerprint will be attached with one distance value DT_{DC}. FT_2 fingerprints will be attached with five distance values DT_{LR}, DT_{LX}, DT_{LI}, DT_{RX}, and DT_{RI}, where DT_{LR} is the distance between two delta points. The large distance from the left (right) delta point to the cores is kept in DT_{LX} (DT_{RX}) and the small one is kept in DT_{LI} (DT_{RI}). FT_3 fingerprints will be attached with seven distance values including the five defined in FT_2 and the distance from left (right) delta point to the centre delta DT_{LD} (DT_{RD}.). Table 3 summarises the attached distance values for each class.

Table 3 Attached distance values for each class

Type	*Attached distance values*
FT_0	{ }
FT_1	$\{DT_{DC}\}$
FT_2	$\{DT_{LR}, DT_{LX}, DT_{LI}, DT_{RX}, DT_{RI}\}$
FT_3	$\{DT_{LR}, DT_{LX}, DT_{LD}, DT_{LI}, DT_{RX}, DT_{RD}, DT_{RI}\}$

While building a fingerprint database, it is reasonable to assume that a clear image will be acquired from the individual. In other words, FT_2 and FT_3 fingerprints in the database should have five and seven distance values calculated from both bottom-left and bottom-right delta points. Therefore, when we search for a particular fingerprint acquired from a crime scene with only a portion of the image with only one delta and one core point, a large number of images in the database can still be ruled out by the remaining valid distance values. The sub-classification scheme can be achieved in two ways: distance-oriented or percentage-oriented described in the following subsection.

5.1 Experiments

The distance of SPs is measured by pixels, which is not discrete data and therefore can be used to further divide each type into subclasses with smaller numbers of images. In order to illustrate this concept, we calculate the distance between SPs (DT_{DC}) in the 2138 properly classified fingerprints in FT_1. These fingerprints are sorted by the DT_{DC} and then relabelled from numbers 1 to 2138. The X-axis in Figure 12(a) is the new fingerprint numbers and Y-axis shows the DT_{DC} in pixels. Roughly speaking, the DT_{DC} is uniformly distributed, and over 90% of DT_{DC} are within 200 pixels (or 26 times the average ridge-valley width).

Figure 12 (a) shows the range of DT_{DC} is from 10 to 295 pixels, and (b) shows the number of fingerprints with the same rounded DT_{DC}

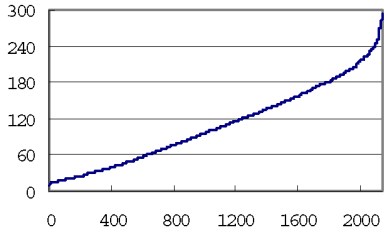

(a)

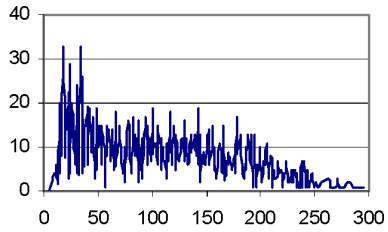

(b)

By rounding DT_{DC}, we count the number of fingerprints (Y-axis) with the same distance (X-axis) as shown in Figure 12(b). The maximum occurrence for the same rounded DT_{DC} is 34 where the X-axis is 18 (2.4 times the average ridge-valley width). Fingerprints in FT_1 can be further divided into subclasses based on DT_{DC} or percentage of occurrences. For instance, in the distance-oriented approach, one can create a subclass for every 60 pixels in distance. Figure 12(a) will then be divided into five subclasses from distance 0 to 300. If we wish to use the distance-oriented approach to make the subclass in the FT_1 account for the same percentage as FT_0 (4%), then Figure 12(a) will be divided into 14 subclasses and each subclass will contain 160 images. A similar sub-classification scheme can be applied to FT_2 and FT_3, which can be divided into more subclasses since they have more distance values.

6 Conclusions

The original SEA suffers from two problems: *the valid singular point disappearing problem* and *the narrow arch*

anomaly. The ESEA presented in this paper successfully overcomes these two problems. ESEA properly locates SPs on fingerprints in a 2×2 pixel area and recognise the type of SP by analysing directional sequence on pixel-wised directional images. According to the type and number of SPs, fingerprints will be assigned to one of the four types FT_0, FT_1, FT_2, and FT_3 with a set of SP distance values. Experimental results show the accuracy rate of ESEA increases 32.5% compared to the SEA and reaches 94.7% on the NIST-4 database. Distance among SPs provide evenly distributed non-discrete information which is used as sub-classification basis to further group fingerprints into subclasses with smaller numbers of occurrences. The search for a specific fingerprint can therefore be performed on specific subclasses containing only a small portion of a large fingerprint database, which will then save enormous computational time. The sub-classification scheme is illustrated by the FT_1 type.

Acknowledgements

This research was supported in part by NSC grant 96-2221-E-033-052.

References

Bolle, R.M., Senior, A.W., Ratha, N.K. and Pankanti, S. (2002) 'Fingerprint minutiae: a constructive definition', *Proc. Int'l Eccv Workshop*, Copenhagen, Denmark, pp.58–66.

Cappelli, R., Lumini, A., Maio, D. and Maltoni, D. (1999) 'Fingerprint classification by directional image partitioning', *IEEE Trans. on PAMI*, Vol. 21, No. 5, pp.402–421.

Federal Bureau of Investigation (1984) *The Science of Fingerprints: Classification and Uses*, US Government Printing Office, Washington DC, USA.

Grasselli, A. (1969) 'On the automatic classification of fingerprints-some consideration on the linguistic interpretation of picture', *Methodologies of Pattern Recognition*, Academic Press, New York.

Henry, E.R. (1900) *Classification and Use of Fingerprints*, Routledge, London.

Hong, L., Wan, Y. and Jain, A.K. (1998) 'Fingerprint image enhancement: algorithm and performance evaluation', *IEEE Trans. on PAMI*, Vol. 20, pp.777–789.

Huang, C.Y., Liu, L.M. and Hung, D.C.D. (2007) 'Fingerprint analysis and singular point detection', *Pattern Recognition Letters*, doi: 10.1016/j.patrec.2007.04.003.

Jain, A.K., Prabhakar, S. and Hong, L. (1999) 'A multichannel approach to fingerprint classification', *IEEE Tran. on PAMI*, Vol. 21, No. 4, pp.348–359.

Jain, A.K. and Minut, S. (2002) 'Hierarchical kernel fitting for fingerprint classification and alignment', *Proceeding of ICPR*, Vol. 2, pp.469–473.

Karu, K. and Jain, A.K. (1996) 'Fingerprint classification', *Patt. Recog.*, Vol. 29, pp.389–404.

Kawagoe, M. and Tojo, A. (1984) 'Fingerprint pattern classification', *Patt. Recog.*, Vol. 17, No. 3, pp.295–303.

Marcialis, G., Roli, F. and Frasconi, P. (2001) 'Fingerprint classification by combination of flat and structural approaches', in Bigun J. and Smeraldi, F. (Eds.): *Proc. AVBPA*, *LNCS* 2091, Springer, Halmstad, Sweden, pp.241–246.

Neto, H.V. and Borges, D.L. (1997) 'Fingerprint classification with neural networks', *Proc. 4th Brazilian Symposium on Neural Networks*, IEEE CS Press, Goiânia, Brazil, pp.66–72.

Senior, A.W. (2001) 'A combination fingerprint classifier', *IEEE Trans. on PAMI*, Vol. 23, No. 10, pp.1165–1174.

Sherlock, B.G. and Monro, D.M. (1993) 'A model for interpreting fingerprint topology', *Patt. Recog.*, Vol. 26, No. 7, pp.1047–1055.

Srinivasan, V.S. and Murthy, N.N. (1992) 'Detection of singular points in fingerprint images', *Patt. Recog*., Vol. 25, No. 2, pp.139–153.

Tan, X., Bhanu, B. and Lin, Y. (2003) 'Learning features for fingerprint classification', *Proceedings International Conference on Audio- and Video-based Biometric Person Authentication*, Guildford, UK, pp.318–326.

Watson, C.I. and Wilson, C.L. (1992) *NIST Special Database 4, Fingerprint Database*, National Institute of Standards and Technology.

Yao, Y., Marcialis, G., Pontil, M., Frasconi, P. and Roli, F. (2003) 'Combining flat and structured representations for fingerprint classification with recursive neural networks and support vector machines', *Patt. Recog*., Vol. 36, No. 2, pp.397–406.